Comparison of Simultaneously Measured Perfusion and BOLD Signal Increases During Brain Activation With T_1-Based Tissue Identification

Wen-Ming Luh,[1,2]* Eric C. Wong,[2,3] Peter A. Bandettini,[1] B. Douglas Ward,[1] and James S. Hyde[1]

Perfusion and blood oxygenation level-dependent (BOLD) signals were simultaneously measured during a finger-tapping task at 3T using QUIPSS II with thin-slice TI$_1$ periodic saturation, a modified pulsed arterial spin labeling technique that provides quantitative measurement of perfusion. Perfusion and BOLD signal changes due to motor activation were obtained and correlated with the T_1 values estimated from echo-planar imaging (EPI)-based T_1 maps on a voxel-by-voxel basis. The peak perfusion signal occurs in voxels with a T_1 of brain parenchyma while the peak BOLD signal occurs in voxels with a T_1 characteristic of blood and cerebrospinal fluid. The locations of the peak signals of functional BOLD and perfusion only partially overlap on the order of 40%. Perfusion activation maps will likely represent the sites of neuronal activity better than do BOLD activation maps. Magn Reson Med 44:137–143, 2000. © 2000 Wiley-Liss, Inc.

Key words: perfusion; BOLD; arterial spin labeling; T_1 map

In addition to obtaining resting-state images of cerebral blood flow (CBF), magnetic resonance imaging (MRI)-based arterial spin labeling (ASL) techniques (1–18), using water protons in arterial blood as freely diffusible tracers, can be applied to map brain function. ASL techniques employ a different physiological principle than do blood oxygenation level-dependent (BOLD) contrast techniques (19–21). Due to differences in the contrast mechanisms underlying ASL and BOLD, it is expected that the spatial location of functional signal from these techniques will be different. Many studies have shown that much of the BOLD signal originates from macroscopic veins (22–24). In contrast, the amount of ASL signal in the veins is negligible (15). Nevertheless, Siewert et al. (9) showed that no significant difference was found for the d-prime between BOLD and echo-planar imaging and signal targeting with alternating radio frequency (EPISTAR; 7–9). Kim et al. (12) have reported that some activation areas can only be detected by flow-sensitive alternating inversion recovery (FAIR; 10–14), but not BOLD. With sufficient spatial resolution, activation maps created using ASL and BOLD techniques should show different spatial distributions. We hypothesize that ASL techniques will provide better localization of the sites of neuronal activity than do BOLD techniques.

The BOLD signal reflects changes of several parameters, including cerebral blood volume, CBF, and oxygen extraction. Experimental measurement of CBF along with the BOLD signal can provide information that brings us toward a quantitative understanding of the mechanism of the BOLD signal (25).

Both continuous and pulsed ASL techniques have previously been applied to functional brain imaging (4–9,11–15). Pulsed ASL techniques generally have a better achievable temporal resolution than do continuous methods (typical TR of 2 sec vs. 4 sec). A recent study (17) showed that the signal-to-noise ratios (SNRs) per unit time of both techniques using transit delay insensitive continuous and pulsed techniques (3,16) are very similar. Studies using conventional pulsed ASL techniques, such as EPISTAR and FAIR, are subject to systematic errors due to transit delay and "flow-through" effect (15,16). Quantitative imaging of perfusion using a single subtraction, second version (QUIPSS II; 15–17) is a modified pulsed ASL technique that is insensitive to systematic errors due to transit delay and flow-through effect. QUIPSS II with thin-slice TI$_1$ periodic saturation (Q2TIPS; 18), used in the present study, is a modified version of QUIPSS II which minimizes residual errors due to the mismatch between the slice profile of the QUIPSS II saturation pulse and that of the inversion tagging pulse.

One advantage of the pulsed ASL pulse sequences is the ability to measure perfusion and BOLD signals simultaneously by the application of in-plane saturation pulses in the imaging slice immediately before the inversion pulse (15,16). The magnetization of tagged blood undergoes inversion recovery during the tag state and is fully relaxed during the control state, while the magnetization of static tissues undergoes saturation recovery during both states. The subtraction of tag-state signal from control-state signal results in a perfusion-weighted signal, and the addition of signal of both states results in BOLD-weighted signal. Compared to acquiring perfusion and BOLD data separately, this acquisition scheme shortens the scanning time by half and eliminates the possibility of misregistration between time series acquired separately.

Herein we apply Q2TIPS to functional motor activation studies to simultaneously measure CBF and BOLD signals. The signal changes due to task activation were correlated to the T_1 values from echo-planar imaging (EPI)-based T_1 maps obtained in the same sessions to help identify the

---

[1]Biophysics Research Institute, Medical College of Wisconsin, Milwaukee, Wisconsin.

[2]Department of Radiology, University of California at San Diego, La Jolla, California.

[3]Department of Psychiatry, University of California at San Diego, La Jolla, California.

*Correspondence to: Wen-Ming Luh, Ph.D., UCSD Thornton Hospital, Radiology MC-7756, 9300 Campus Point Drive, La Jolla, CA 92037. E-mail: wmluh@ucsd.edu

type of tissue present in each voxel. The aim of this study is to compare the spatial distribution and the changes of CBF and BOLD signals during finger-tapping episodes, and to use local T_1 values to identify the tissues that give rise to these signals.

MATERIALS AND METHODS

Functional MRI

Studies were performed using a 3T Bruker Biospec 30/60 scanner (Bruker Medical, Karlsruhe, Germany) fitted with a three-axis local head gradient coil and an endcapped quadrature birdcage coil. Proximal inversion with a control for off-resonance effects (PICORE; 15) was used with Q2TIPS, as implemented by Luh et al. (18). The Q2TIPS saturation pulses were periodically applied from time TI_1 to TI_{1S} (TI_1 stop time) every 25 msec in a 2-cm thick periodic saturation slice; the images were acquired at time TI_2. Subjects were instructed to perform self-paced bilateral finger tapping with sequential thumb-to-digit oppositions. Each run consisted of an initial 10-TR rest period followed by five repetitions of a 20-TR task period and a 30-TR rest period. To optimize TI_1 for functional studies, TI_1 should be as long as possible to maximize SNR but shorter than the shortest temporal width of the tag (τ) to control the size of the tag (15–17). To estimate the optimal TI_1, TI_1 was varied from 400 to 800 msec in one subject. Other imaging parameters were: TR = 2.5 sec, field of view (FOV) = 24 cm, slice thickness = 8 mm, matrix size = 64×64, and bandwidth = 125 kHz. TI_2 was 1400 msec to minimize the flow-through effect while maintaining adequate SNR (17). TI_{1S} was empirically set to 1225 msec so that the remaining part of the tagged blood in the tagged region at time TI_1 was completely saturated (18). For the simultaneous perfusion/BOLD experiments, five volunteers (ages 23–34, mean 28.2 years) were studied after giving informed consent. Each volunteer performed five runs of the bilateral finger-tapping paradigm with TI_1 = 700 msec (see Results section), TI_2 = 1400 msec, FOV = 16 cm with matrix size = 64×64 for a nominal in-plane resolution of 2.5 mm $\times$ 2.5 mm, slice thickness = 8 mm, and bandwidth = 125 kHz. TI_{1S} and TR were 1050 msec and 2.3 sec, respectively, as determined experimentally (18) to optimize the SNR per unit time.

EPI-Based T_1 Maps

For the purpose of generating a T_1 map for each subject, 24 inversion recovery (IR)-EPI images of the same motor-cortex slice were acquired immediately prior to the simultaneous perfusion/BOLD studies with the inversion time (TI) increased logarithmically from 30 to 9580 msec and TR = 10 sec. The same adiabatic inversion pulse was used as in PICORE but without slice-selective gradients. IR-EPI provided a fast and accurate way to obtain T_1 maps which can be easily registered to the corresponding perfusion/BOLD activation maps obtained from the Q2TIPS experiments on a voxel-wise basis since they were acquired with the same EPI readout. To estimate the typical T_1 values of white matter (WM), gray matter (GM), and cerebrospinal fluid (CSF) using IR-EPI, four of the subjects were studied with a 2-mm axial slice across ventricles to include more

CSF and reduce partial voluming between tissues. Under these conditions, a simple histogram of T_1 values demonstrates three distinct peaks that correspond to WM, GM, and CSF.

Prior to image reconstruction of the IR-EPI raw data, the complex k-space data with longest TI value was subtracted from the k-space data at each TI value on a point-by-point basis (26). The resulting data can then be magnitude reconstructed, and represent the difference between each TI point and the last TI point. This avoids problems in the T_1 fitting procedure due to the sign inversion of the signal at early TI values, and is essentially the same as using the longest TI image as a phase reference. The reconstructed images were registered to the image to which the Q2TIPS raw images were registered (see Data Processing section) for bulk motion correction using the *imreg* program from the AFNI software package (27). Registered images were then fitted to a single exponential decay curve on a voxel-by-voxel basis by using the nonlinear least-squares regression routines from the AFNI software package.

A histogram of T_1 values was generated from all brain area voxels across four subjects with a 1-msec bin size. After applying a running average of a 21-msec window, the resultant histogram was fitted to the sum of three Gaussian functions to estimate the T_1 values of WM, GM, and CSF.

Volume Fraction and T_1

To estimate the tissue composition of each voxel from measured T_1 values, a computer simulation was performed by constructing the signal intensity versus TI for voxels consisting of different fractions of two tissues (either WM and GM, or GM and CSF). These synthesized data were fitted using the single exponential fitting procedure described above, resulting in an estimate of apparent T_1 as a function of voxel composition.

Data Processing

The first eight Q2TIPS raw images from each run were discarded to ensure that steady state was reached. The remaining raw images were registered to the first image for bulk motion correction using the *imreg* program from the AFNI software package.

For the estimation of the optimal TI_1 value, perfusion time series were first generated by subtracting each image from the two nearest neighbor images in the time series (15). A one-cycle perfusion time series was obtained by averaging each cycle perfusion series with one task/rest period into one cycle. Cross-correlation (28) with an ideal trapezoidal waveform was performed on the one-cycle perfusion time series to identify activated pixels with a correlation coefficient > 0.75. Signals of the activated voxels were averaged from each task and rest period in the perfusion time series. Standard errors were calculated from the variance of the averaged signals of the activated voxels from the perfusion time series during task and rest states, respectively.

For the simultaneous perfusion/BOLD studies, the baseline drift in each run was first removed by fitting the baseline to a fourth-order polynomial function. After grouping all five runs into one time series, the global linear

trend was removed with another polynomial fit. To minimize the BOLD weighting in the perfusion data during transitions of task and rest periods, perfusion time series were constructed by subtracting from each image the average of the previous and the next images in the time series (15). BOLD time series were obtained by adding to each image the average of the previous and the next images in the time series.

Activation and baseline images were chosen after the signal stabilized. For calculating signal changes, images obtained during transitions were excluded, typically within 10 sec after the onset of the task and up to 23 sec after the cessation of the task. For the calculation of BOLD signal changes, images during rest periods with post-stimulus undershoot signal in the BOLD time series were excluded, typically from 10 to 30 sec after the cessation of the task. Resting-state perfusion maps were obtained by averaging all baseline images in the perfusion time series. One-sided Student's t-tests were performed for each voxel between activation and baseline images to generate t-score images. A region of interest (ROI) was selected for each subject that included primary sensorimotor, premotor, and supplementary motor cortex regions. Relative BOLD signal changes ($\Delta BOLD = (S_{Bt} - S_{Br})/S_{Br}$, where S_{Bt} and S_{Br} are the averaged BOLD signals during task and rest periods, respectively) were calculated in voxels with a Bonferroni corrected significance threshold of $P < 0.05$ that corresponds to a probability value of $P < 1.22 \times 10^{-4}$ (0.05/410) for a typical ROI of 410 voxels. Voxels with t-scores above the corresponding cutoff threshold ($t_{.05}$) are considered significantly activated. Absolute perfusion signal changes
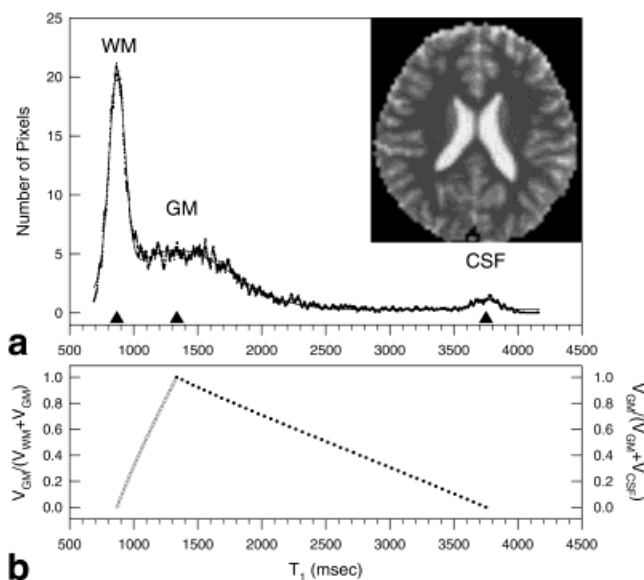

FIG. 2. Averaged Q2TIPS difference signals of the activated voxels during task and rest states as a function of TI_1.

($\Delta CBF = S_{Pt} - S_{Pr}$, where S_{Pt} and S_{Pr} are the calculated perfusion signals during task and rest periods, respectively) were calculated in voxels with t-scores above $t_{.05}$. Perfusion calculations were performed as in a previous study (18).

To evaluate the different spatial distribution of functional signals between BOLD and perfusion, both t-score thresholds were adjusted to realize the same number of activated voxels over a range of voxel numbers (from 8 to 150) for each subject, and the fractional overlap was calculated by dividing the number of overlap voxels with the total number of activated voxels. Futhermore, the overlap percentages were also calculated between each individual run of BOLD time series for each subject. This is a measurement of noise in the overlap between BOLD runs and is used as a reference against which to compare the overlap between BOLD and perfusion. For each number of activated voxels (corresponding to different t-score thresholds for BOLD and perfusion), mean T_1 values were calculated from the BOLD-activated, perfusion-activated, and overlapping voxels, respectively.

RESULTS

The histogram (dotted line) of four T_1 maps and the fitted curve (solid line) are shown in Fig. 1a, along with a representative T_1 map through ventricles. Fig. 1b shows the simulation results of volume fraction and T_1 values. The estimated T_1 values (solid triangles) of WM, GM, and CSF are 870 ± 62, 1338 ± 430, and 3752 ± 88 msec (mean ± SD), respectively. The estimated mean values are consistent with those determined by conventional methods (29). WM and CSF have a much smaller standard deviation than GM, indicating that WM and CSF are mostly uniform within voxels in the T_1 maps with a nominal voxel size of $2.5 \times 2.5 \times 2$ mm^3. Assuming that each voxel consists of only two types of tissue, either GM/WM (open circles) or GM/CSF (closed circles), the fitted T_1 values exhibit a nearly linear dependence on volume fraction.

To estimate the optimal TI_1 value for functional studies, the averaged Q2TIPS signals of task and rest states as a function of TI_1 from activated voxels are plotted in Fig. 2. The Q2TIPS signals during the rest state exhibit a linear dependence on TI_1 while the Q2TIPS signals during the

FIG. 1. **a:** Histogram (dotted line) of T_1 maps with voxel size of $2.5 \times 2.5 \times 2$ mm^3 after applying a 21-msec running-average window and the fitted curve (solid line) of the sum of three Gaussian functions. The estimated T_1 values (solid triangles) of WM, GM, and CSF are 870 ± 62, 1338 ± 430, and 3752 ± 88 msec (mean ± SD), respectively. The insert image represents one of the T_1 maps used to generate the histogram. **b:** Volume fraction of GM mixed with WM (open circles) and with CSF (solid circles) as a function of fitted T_1 values, using computer simulation.
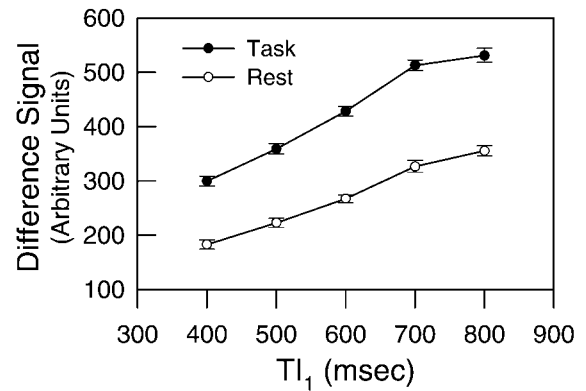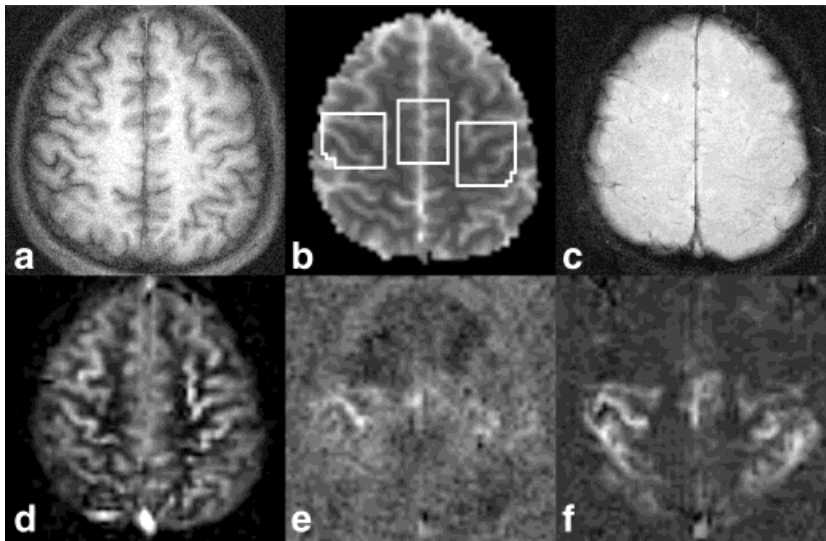
FIG. 3. **a:** Anatomical reference image, **b:** T_1 map (selected ROI is shown), **c:** T_2^*-weighted image, **d:** Resting-state perfusion map, **e:** Perfusion t-score image, and **f:** BOLD t-score image. Activated voxels were obtained by thresholding the t-score images.

task state deviate from the linear dependence at $TI_1 = 700$ msec. This indicates that τ is about 700 msec during the task state. In previous work, we measured τ to be about 900 msec at rest (18). To be quantitative, TI_1 should be shorter than the shorter τ between task and rest states. Therefore, $TI_1 = 700$ msec was used in the present perfusion/BOLD study.

Figure 3 shows the anatomical reference image, T_1 map, T_2^*-weighted FLASH image (flip angle = 45°, TE = 30 msec, TR = 300 msec), quantitative resting-state perfusion map, and t-score images of perfusion and BOLD activation maps from a representative subject. Activated voxels were obtained by thresholding the t-score images. The SNR of the activation signals were much higher in BOLD than perfusion activation maps. On average, 2.7 times more voxels in the BOLD activation maps than in the perfusion activation maps were significantly activated within the ROIs with t-scores above $t_{.05}$.

Calculated absolute CBF values of the voxels in the ROI versus T_1 from the resting-state perfusion map in Fig. 3d are shown in Fig. 4. The CBF values in the majority of the voxels with T_1 values smaller than 1500 msec show a linear dependence on T_1 (correlation coefficient $r = 0.77$). This suggests that the measured perfusion signal is proportional to $V_{GM}/(V_{WM}+V_{GM})$ where V_{GM} and V_{WM} are the volumes of GM and WM, respectively. The largest CBF values were located in the voxels with T_1 values around 1800 msec. The CBF values of the voxels with T_1 values larger than 1800 msec show another linear dependence on T_1 ($r = -0.65$), suggesting again that CBF is proportional to the GM fraction $V_{GM}/(V_{GM}+V_{CSF})$ where V_{CSF} is the volume of CSF. These same phenomena (positive correlation at low T_1, negative correlation at high T_1) were observed in all other subjects (data not shown).

Figure 5a,b shows ΔCBF and ΔBOLD versus T_1 of voxels with t-scores above $t_{.05}$ in the corresponding perfusion and BOLD activation maps from all subjects. In the BOLD activation maps, 819 voxels ($T_1 = 1548 \pm 502$ msec and ΔBOLD $= 0.9 \pm 0.9$ %, mean $\pm$ SD) out of 1229 voxels ($T_1 = 1535 \pm 464$ msec and ΔBOLD $= 1.1 \pm 1.0$ %) do not show activation in the perfusion signal, especially those

voxels with long T_1 values. Most voxels with T_1 values ranging from 900 to 1500 msec possess ΔBOLD values less than 2%. In the perfusion activation maps, only 49 voxels ($T_1 = 1190 \pm 246$ msec and ΔCBF $= 17 \pm 6$ ml/100 ml/min) out of 459 voxels ($T_1 = 1477 \pm 376$ msec and ΔCBF $= 25 \pm 13$ ml/100 ml/min) do not exhibit significant activation in the BOLD activation maps. Based on the T_1 values, these voxels are mostly at the border between GM and WM, and are therefore less likely to contain large veins. The other 89% of voxels in the perfusion activation maps are also activated in the BOLD activation maps. Large ΔCBF values are observed predominantly in the voxels with T_1 values around the estimated T_1 value of GM (1338 $\pm$ 430 msec). The ΔCBF vs. T_1 data indicate that low T_1 tissues are involved in the perfusion signal change. Large ΔBOLD values are much more widely distributed
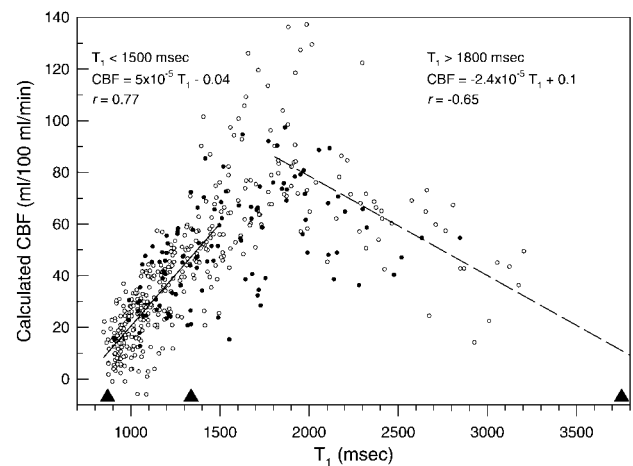

FIG. 4. Calculated CBF from voxels in the ROI in the resting-state perfusion image (Fig. 3d) as a function of T_1. Black circles: The voxels with significant activation with $P < 0.05$ (Bonferroni corrected) in both perfusion and BOLD activation maps. Solid triangles, left to right: The estimated mean T_1 values of WM, GM, and CSF, respectively. Fitted equations and r values are shown for voxels with T_1 values less than 1500 msec and larger than 1800 msec.
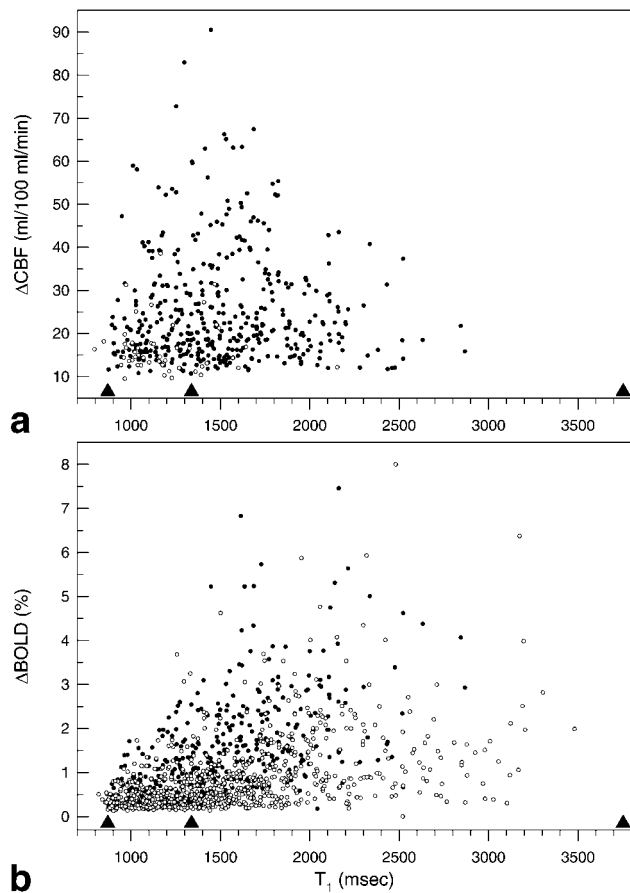
FIG. 5. ΔCBF (**a**) and ΔBOLD (**b**) of statistically significant activated voxels from all subjects as a function of T_1. Black circles: The voxels with significant activation in both perfusion and BOLD activation maps. Solid triangles, left to right: The estimated mean T_1 values of WM, GM, and CSF, respectively.

DISCUSSION

EPI-based T_1 maps provide a means of tissue identification and allow direct comparison with EPI-based perfusion and BOLD activation maps on a voxel-wise basis. Blood is known to have a slightly higher T_1 than does GM (30,31), but because very few voxels contain predominantly blood, the blood signal does not appear as a separate peak on the T_1 histogram (Fig. 1). The average thickness of GM is about 2.5 mm and the motor cortex is usually the thickest (∼ 3.5–4.5 mm) (32). With a nominal voxel size of $2.5 \times 2.5 \times 8$ mm^3, most voxels that contain GM will also contain other tissues. Because WM and CSF lie on opposite sides of the cortical ribbon, we assumed here that voxels near the cortex contain either GM and CSF or GM and WM. With this simplifying two-tissue assumption, the T_1 value should indicate both the major tissue components in a voxel and their volume fractions.

EPI-based T_1 maps provide an independent means of identifying voxels which may exhibit similar measurable parameters such as CBF, or BOLD. This type of information can be used in conjunction with the selection of ROIs based on spatial proximity or anatomical landmarks. Other information, such as T_2/T_2^* maps and apparent diffusion
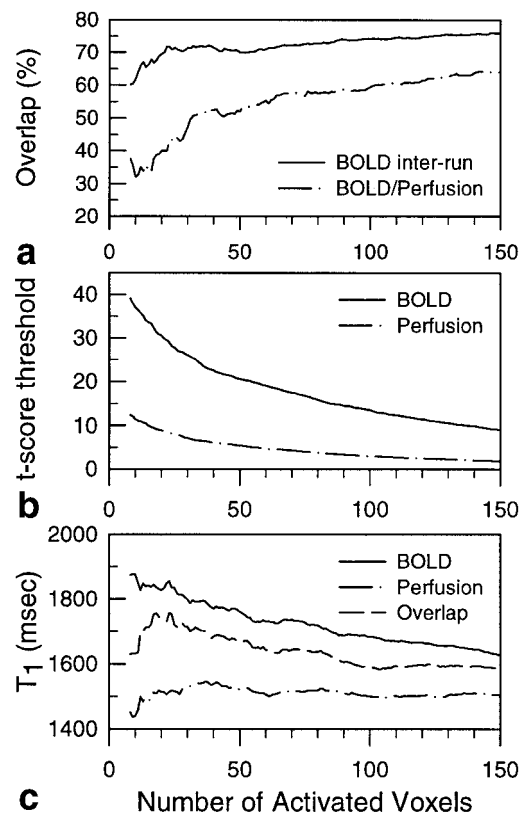
across the T_1 range than ΔCBF, with peak ΔBOLD occurring at T_1 values between the estimated T_1 values of GM and CSF.

The overlap percentage of functional BOLD and perfusion signals is shown in Fig. 6a averaged from all subjects, together with the overlap percentage between individual BOLD runs. Figure 6b shows the averaged *t*-score thresholds used to obtain a certain number of activated voxels for BOLD and perfusion, respectively. As the number of activated voxels decreases, the overlap ratio generally decreases while the overlap percentage between each individual BOLD run is on the order of 70% across most voxel numbers, due to the variability between runs. This indicates that the locations of the peak signals of functional BOLD and perfusion only partially overlap on the order of 40%. Figure 6c shows the mean T_1 values of the activated voxels from BOLD and perfusion activation maps, and from the overlap voxels. The mean T_1 values from BOLD-activated voxels generally increase as the overall voxel number decreases, indicating that the largest BOLD signals come from voxels that include CSF and/or blood. The mean T_1 values of perfusion-activated voxels, however, stay close to the GM T_1 values as the voxels number decreases.

FIG. 6. **a:** Averaged overlap percentage between BOLD and perfusion maps, and between individual BOLD runs across all subjects. **b:** Averaged BOLD and perfusion *t*-score thresholds used to obtain the desired number of activated voxels for the overlap percentage between BOLD and perfusion maps. **c:** Mean T_1 values of BOLD-activated, perfusion-activated, and overlap voxels across all subjects with matched total number of activated voxels by varying the *t*-score thresholds.

coefficient maps, may also be useful for tissue segmentation if easily obtained and registered. The tissue constituents in each voxel can be obtained (perhaps with greater accuracy) using images with multiple forms of contrast (33). However, it is important to note that the T_1 method used in this study is rapid and contains identical spatial distortions to the functional images, allowing for acquisition of a T_1-based tissue map with each functional study without the need for distortion correction or across-study image registration.

Q2TIPS provides quantitative measurement of perfusion and perfusion changes, simultaneous measurement of BOLD contrast, compensation of transit delay errors, minimization of the flow-through effect and venous tagged blood contribution, and improved TI_1 saturation (18). For a localized area such as the motor cortex, the transit delay may be similar among voxels. However, the transit delay even *within* a voxel changes dynamically with functional activation (34,35).

In this study, the BOLD signal was obtained from the sum of the tag and control images. Because the T_1 value of blood is longer than brain tissues, this approach introduces some negative weighting on the BOLD signal compared to conventional BOLD technique (15). The Q2TIPS saturation pulses cause the tail of the tagged blood to return to fully relaxed state at a later time than using non-QUIPSS–based techniques, resulting a slightly more negative flow weighting on the BOLD signal. This results in a reduction in the BOLD signal that is on the order of 15% relative to conventional BOLD measurements (data not shown). We are currently investigating the relative spatial distributions of BOLD signals derived from Q2TIPS and conventional BOLD techniques.

It is known that BOLD signals contain a large contribution from draining veins and contain both intravascular and extravascular components (23,24). In this study large ΔBOLD values were seen to occur in voxels with a broad range of T_1 values. It thus appears that large ΔBOLD values may occur in any kind of tissues as long as they are surrounded by veins draining from the activation sites, and that the BOLD signal is not well localized to GM.

Using the same statistical threshold, the number of BOLD-activated voxels is much greater than that of perfusion-activated voxels due to the higher SNR of the BOLD signal. The averaged ΔBOLD and ΔCBF values can vary several fold as the statistical threshold changes. Therefore, caution must be exercised when comparing averaged values of resting-state perfusion, ΔCBF, or ΔBOLD, with literature values and with data obtained with other modalities, such as positron emission tomography. By changing the thresholds of both BOLD and perfusion activation maps to match the total number of activated voxels, our data suggest that the location of the peak perfusion signal change is in general not in the same location as the peak of the BOLD signal change. It has been noted anecdotally by many investigators that the ASL and BOLD functional signals only partially overlap in space. The data shown here demonstrates quantitatively that the overlap is on the order of 40% for voxels with high *t*-scores, and indicates that the BOLD signal contains a larger contribution from CSF and/or blood containing voxels. This is as expected, since the draining veins, including intracortical and pial veins, are surrounded by CSF, while there has been no rationale set forth for a contribution to the ASL signal from CSF.

Brain tissue that receives increased perfusion is presumably the site of neuronal activity itself. Our data suggest that perfusion activation maps better localize the sites of neuronal activity than do BOLD activation maps. Although it is possible to acquire the larger BOLD signal, and subsequently select only GM voxels, it is still difficult to determine whether the BOLD signal is intrinsic to those GM voxels or is due to nearby draining veins.

CONCLUSIONS

Correlation of T_1 maps, BOLD, and CBF signals on a voxelwise basis provides information about the tissues that give rise to these functional signals. Perfusion activation maps are clearly better localized to brain parenchyma, and will likely represent the sites of neuronal activity better than do BOLD activation maps.

ACKNOWLEDGMENTS

REFERENCES

1. Williams DS, Detre JA, Leigh JS, Koretsky AP. Magnetic resonance imaging of perfusion using spin inversion of arterial water. Proc Natl Acad Sci USA 1992;89:212–216.
2. Detre JA, Leigh JS, Williams DS, Koretsky AP. Perfusion imaging. Magn Reson Med 1992;23:37–45.
3. Alsop DC, Maccotta L, Detre JA. Multi-slice perfusion imaging using adiabatic arterial spin labeling and an amplitude modulated control. In: Proceedings of the 5th Annual Meeting of the ISMRM, Vancouver, 1997. p 81.
4. Ye FQ, Smith AM, Yang Y, Duyn J, Mattay VS, Ruttimann UE, Frank JA, Weinberger DR, McLaughlin AC. Quantification of regional cerebral blood flow increases during motor activation: a steady-state arterial spin tagging study. Neuroimage 1997;6:104–112.
5. Talagala SL, Noll DC. Functional MRI using steady-state arterial water labeling. Magn Reson Med 1998;39:179–183.
6. Bock C, Schmitz B, Kerskens CM, Gyngell ML, Hossmann K-A, Hoehn-Berlage M. Functional MRI of somatosensory activation in rat: effect of hypercapnic up-regulation on perfusion- and BOLD-imaging. Magn Reson Med 1998;39:457–461.
7. Edelman RR, Siewert B, Darby DG, Thangaraj V, Nobre AC, Mesulam MM, Warach S. Qualitative mapping of cerebral blood flow and functional localization with echo-planar MR imaging and signal targeting with alternating radio frequency. Radiology 1994;192:513–520.
8. Edelman RR, Wielopolski P, Schmitt F. Echo-planar MR imaging. Radiology 1994;192:600–612.
9. Siewert B, Bly BM, Schlaug G, Darby DG, Thangaraj V, Warach S, Edelman RR. Comparison of the BOLD- and EPISTAR-technique for functional brain imaging by using signal detection theory. Magn Reson Med 1996;36:249–255.
10. Kwong KK, Chesler DA, Weisskoff RM, Rosen BR. Perfusion MR imaging. In: Proceedings of the 2nd Annual Meeting of the SMR, San Francisco, 1994. p 1005.
11. Kim S-G. Quantification of relative cerebral blood flow change by flow-sensitive alternating inversion recovery (FAIR) technique: application to functional mapping. Magn Reson Med 1995;34:293–301.
12. Kim S-G, Tsekos NV. Perfusion imaging by a flow-sensitive alternating inversion recovery (FAIR) technique: application to functional brain imaging. Magn Reson Med 1997;37:425–435.

13. Kim S-G, Ugurbil K. Comparison of blood oxygenation and cerebral blood flow effects in fMRI: estimation of relative oxygen consumption change. Magn Reson Med 1997;38:59–65.

14. Davis TL, Kwong KK, Weisskoff RM, Rosen BR. Calibrated functional MRI: mapping the dynamics of oxidative metabolism. Proc Natl Acad Sci USA 1998;95:1834–1839.

15. Wong EC, Buxton RB, Frank LR. Implementation of quantitative perfusion imaging techniques for functional brain mapping using pulsed arterial spin labeling. NMR Biomed 1997;10:237–249.

16. Wong EC, Buxton RB, Frank LR. Quantitative imaging of perfusion using a single subtraction (QUIPSS and QUIPSS II). Magn Reson Med 1998;39:702–708.

17. Wong EC, Buxton RB, Frank LR. A theoretical and experimental comparison of continuous and pulsed arterial spin labeling techniques for quantitative perfusion imaging. Magn Reson Med 1998;40:348–355.

18. Luh W-M, Wong EC, Bandettini PA, Hyde JS. QUIPSS II with thin-slice TI_1 periodic saturation: a method for improving accuracy of quantitative perfusion imaging. Magn Reson Med 1999;41:1246–1254.

19. Bandettini PA, Wong EC, Hinks RS, Tikofsky RS, Hyde JS. Time course EPI of human brain function during task activation. Magn Reson Med 1992;25:390–397.

20. Kwong KK, Belliveau JW, Chesler DA, Goldberg IE, Weisskoff RM, Poncelet BP, Kennedy DN, Hoppel BE, Cohen MS, Turner R, Cheng H-M, Brady TJ, Rosen BR. Dynamic magnetic resonance imaging of human brain activity during primary sensory stimulation. Proc Natl Acad Sci USA 1992;89:5675–5679.

21. Ogawa S, Tank DW, Menon R, Ellermann JM, Kim S-G, Merkle H, Ugurbil K. Intrinsic signal changes accompanying sensory stimulation: functional brain mapping with magnetic resonance imaging. Proc Natl Acad Sci USA 1992; 89:5951–5955.

22. Lai S, Hopkins AL, Haacke EM, Li D, Wasserman BA, Buckley P, Friedman L, Meltzer H, Hedera P, Friedland R. Identification of vascular structures as a major source of signal contrast in high resolution 2D and 3D functional activation imaging of the motor cortex at 1.5T: preliminary results. Magn Reson Med 1993;30:387–392.

23. Boxerman JL, Bandettini PA, Kwong KK, Baker JR, Davis TL, Rosen BR, Weisskoff RM. The intravascular contribution to fMRI signal change: Monte Carlo modeling and diffusion-weighted studies in vivo. Magn Reson Med 1995;34:4–10.

24. Song AW, Wong EC, Tan SG, Hyde JS. Diffusion weighted fMRI at 1.5T. Magn Reson Med 1996;35:155–158.

25. Buxton RB, Wong EC, Frank LR. Dynamics of blood flow and oxygenation changes during brain activation: the balloon model. Magn Reson Med 1998;39:855–864.

26. Kim S-G, Hu X, Ugurbil K. Accurate T_1 determination from inversion recovery images: application to human brain at 4 Tesla. Magn Reson Med 1994;31:445–449.

27. Cox RW. AFNI-software for analysis and visualization of functional magnetic resonance neuroimages. Comput Biomed Res 1996;29:162–173.

28. Bandettini PA, Jesmanowicz A, Wong EC, Hyde JS. Processing strategies for time-course data sets in functional MRI of the human brain. Magn Reson Med 1993;30:161–173.

29. Wansapura JP, Holland SK, Dunn RS, Ball WS. 3.0 Tesla study of NMR relaxation times in the human brain. In: Proceedings of the 5th Annual Meeting of ISMRM, Vancouver, 1997. p 685.

30. Ye FQ, Matay VS, Jezzard P, Frank JA, Weinberger DR, McLaughlin AC. Correction for vascular artifacts in cerebral blood flow values measured by using arterial spin tagging techniques. Magn Reson Med 1997;37: 226–235.

31. Cho S, Jones D, Reddick WE, Ogg RJ, Steen RG. Establishing norms for age-related changes in proton T_1 of human brain tissue in vivo. Magn Reson Imaging 1997;15:1133–1143.

32. Truex RC. Strong and Elwyn's human neuroanatomy. Baltimore: Williams & Wilkins; 1959.

33. Bedell BJ, Narayana PA. Volumetric analysis of white matter, gray matter, and CSF using fractional volume analysis. Magn Reson Med 1998;39:961–969.

34. Buxton RB, Frank LR, Wong EC, Siewert B, Warach S, Edelman RR. A general kinetic model for quantitative perfusion imaging with arterial spin labeling. Magn Reson Med 1998;40:383–396.

35. Luh W-M, Bandettini PA, Hyde JS. Quantification of relative perfusion changes in functional brain imaging using diffusion weighted FAIR: comparison of T_1 model and kinetic model. In: Proceedings of the 6th Annual Meeting of ISMRM, Sydney, 1998. p 1466.